# Exclusive production of proton-antiproton pairs in two-photon collisions

H. Aihara,[n] M. Alston-Garnjost,[a] R. E. Avery,[a] A. Barbaro-Galtieri,[a] A. R. Barker,[g] A. V. Barnes,[a] B. A. Barnett,[j] D. A. Bauer,[g] H.-U. Bengtsson,[d] D. L. Bintinger,[f] G. J. Bobbink,[h] T. S. Bolognese,[a] A. D. Bross,[a] C. D. Buchanan,[d] A. Buijs,[m] M. P. Cain,[b] D. O. Caldwell,[g] A. R. Clark,[a] G. D. Cowan,[a] D. A. Crane,[j] O. I. Dahl,[a] K. A. Derby,[a] J. J. Eastman,[a] P. H. Eberhard,[a] T. K. Edberg,[a] A. M. Eisner,[c] R. Enomoto,[n] F. C. Erné,[m] T. Fujii,[n] J. W. Gary,[a] W. Gorn,[e] J. M. Hauptman,[i] W. Hofmann,[a] J. E. Huth,[a] J. Hylen,[j] T. Kamae,[n] H. S. Kaye,[a] K. H. Kees,[f] R. W. Kenney,[a] L. T. Kerth,[a] Winston Ko,[b] R. I. Koda,[d] R. R. Kofler,[k] K. K. Kwong,[e] R. L. Lander,[b] W. G. J. Langeveld,[e] J. G. Layter,[e] F. L. Linde,[m] C. S. Lindsey,[e] S. C. Loken,[a] A. Lu,[g] X-Q. Lu,[j] G. R. Lynch,[a] R. J. Madaras,[a] K. Maeshima,[b] B. D. Magnuson,[c] J. N. Marx,[a] G. E. Masek,[f] L. G. Mathis,[a] J. A. J. Matthews,[j] S. J. Maxfield,[k] S. O. Melnikoff,[e] E. S. Miller,[f] W. Moses,[a] R. R. McNeil,[b] P. Nemethy,[l] D. R. Nygren,[a] P. J. Oddone,[a] H. P. Paar,[m] D. A. Park,[d] S. K. Park,[i] D. E. Pellett,[b] M. Pripstein,[a] M. T. Ronan,[a] R. R. Ross,[a] F. R. Rouse,[a] K. A. Schwitkis,[g] J. C. Sens,[m] G. Shapiro,[a] M. D. Shapiro,[a] B. C. Shen,[e] W. E. Slater,[d] J. R. Smith,[b] J. S. Steinman,[d] M. L. Stevenson,[a] D. H. Stork,[d] M. G. Strauss,[d] M. K. Sullivan,[c] T. Takahashi,[n] J. R. Thompson,[f] N. Toge,[n] S. Toutounchi,[k] R. van Tyen,[a] B. van Uitert,[m] G. J. VanDalen,[e] R. F. van Daalen Wetters,[d] W. Vernon,[f] W. Wagner,[b] E. M. Wang,[a] Y. X. Wang,[g] M. R. Wayne,[d] W. A. Wenzel,[a] J. T. White,[f] M. C. S. Williams,[b] Z. R. Wolf,[a] H. Yamamoto,[a] S. J. Yellin,[g] C. Zeitlin,[b] and W-M. Zhang[j]

[a]*Lawrence Berkeley Laboratory, Berkeley, California 94720*

[b]*University of California, Davis, California 95616*

[c]*University of California Intercampus Institute for Research at Particle Accelerators, Stanford, California 94305*

[d]*University of California, Los Angeles, California 90024*

[e]*University of California, Riverside, California 92521*

[f]*University of California, San Diego, California 92093*

[g]*University of California, Santa Barbara, California 93106*

[h]*Carnegie-Mellon University, Pittsburgh, Pennsylvania 15213*

[i]*Ames Laboratory, Iowa State University, Ames, Iowa 50011*

[j]*Johns Hopkins University, Baltimore, Maryland 21218*

[k]*University of Massachusetts, Amherst, Massachusetts 01003*

[l]*New York University, New York, New York 10003*

[m]*National Institute for Nuclear and High Energy Physics, Amsterdam, The Netherlands*

[n]*University of Tokyo, Tokyo, Japan*

(TPC/Two-Gamma Collaboration)

(Received 8 May 1987)

We report cross sections for the process $\gamma\gamma \to p\bar{p}$ at center-of-mass energies $W$ from 2.0 to 2.8 GeV. These results have been extracted from measurements of $e^+e^- \to e^+e^-p\bar{p}$ at an overall center-of-mass energy of 29 GeV, using the TPC/Two-Gamma facility at the SLAC storage ring PEP. Cross sections for the untagged mode [both photons nearly real] are shown to lie well above QCD predictions. Results are also presented for the single-tagged mode [one photon in the range $0.16 < Q^2 < 1.6$ (GeV/$c$)$^2$].

Quantum chromodynamics has been used to predict cross sections for the exclusive production of high-transverse-momentum hadron pairs in two-photon collisions. The main ingredients of existing models are nonperturbative hadron wave functions and perturbatively computed amplitudes for the hard scattering of the constituent quarks. Predictions for meson pairs[1] have been approximately borne out by measurements[2-4] of $\gamma\gamma \to \pi^+\pi^-$ and $\gamma\gamma \to K^+K^-$ at center-of-mass energies $W > 1.5$ GeV. For the case of baryon pairs, calculations[5-7] are more difficult and less certain. The calculations of Refs. 5 and 6 differ by more than an order of magnitude in their predicted cross sections when using identical wave functions. A recent calculation[8] for off-shell photons agrees with Ref. 6 in the limit of real photons. Previous measurements[9,10] of $\gamma\gamma \to p\bar{p}$, in the range $2.0 < W < 3.1$ GeV, yielded cross sections well above the predictions of Refs. 6 and 7.

We report here a new measurement of $\gamma\gamma \to p\bar{p}$ for quasireal (untagged) photons with $2.0 < W < 2.8$ GeV and $|\cos\theta^*| < 0.8$, where $\theta^*$ is the scattering angle of the proton or antiproton with respect to the direction of the incoming photons in the $\gamma\gamma$ center of mass. The observed reaction is $e^+e^- \to e^+e^-p\bar{p}$, where both final-

 

state leptons go undetected. We also report the first measurement of this process with one of the photons highly virtual, having a spacelike invariant mass squared $-Q^2$, where $0.16 < Q^2 < 1.6$ $(\mathrm{GeV}/c)^2$. These photons are tagged by detecting one of the final-state leptons. The measurement was carried out using the TPC/Two-Gamma facility[11,12] at the SLAC $e^+e^-$ storage ring PEP, with incident $e^+$ and $e^-$ energies of 14.5 GeV.

The tagged data were collected in two running periods, characterized by differences in the TPC magnetic field and single-tag trigger. The older sample of tagged data corresponds to an integrated luminosity of 54 $\mathrm{pb}^{-1}$ and the newer sample to 38 $\mathrm{pb}^{-1}$. The untagged data are from the earlier period, with an integrated luminosity of 75 $\mathrm{pb}^{-1}$. The Time Projection Chamber (TPC) tracked charged particles in a solenoidal magnetic field. For the old (new) sample, the field strength was 4 (13) kG, with momentum resolution at large angles given given by $\delta p/p \approx 6\%$ (1.5%). The TPC also sampled ionization loss ($dE/dx$) along particle trajectories, with a typical resolution of 3.5%. Tracks from charged particles were recorded in a four-layer inner drift-chamber (IDC) within the TPC pressure vessel and in a three-layer outer drift chamber (ODC) located outside the coil of the solenoid. The IDC and ODC provide azimuthal ($\phi$) information only. Two proportional-mode pole-tip calorimeters (PTC) and a hexagonal Geiger-mode calorimeter (HEX) covered polar angles above 260 mrad. Tagging electrons and positrons were detected in two arrays of NaI crystals in the polar-angle range 25–90 mrad and in lead/scintillator shower counters from 100 to 180 mrad. Charge information was provided by fifteen drift-chamber planes in front of these detectors. The NaI and shower-counter energy resolutions at 14.5 GeV were, respectively, 1.5% and 5% rms.

The trigger for the untagged data required at least two charged tracks in the TPC in different 60° azimuthal sectors, each with polar angle $\theta > 30°$ and projecting to the interaction point within 20 cm along the beam axis. Tracks with $\theta > 45°$ were required to be in coincidence with hits in the ODC within a $\phi$-dependent window which was always at least $\pm 30°$. The ODC requirement limited the trigger efficiency for events with low-momentum tracks because of the presence of the magnet coil and associated material (a total of 1.3 radiation lengths) in front of the ODC. Antiprotons which stopped in the coil annihilated and had a good chance to cause ODC hits, thus contributing to the trigger. This is in contrast with low-momentum protons, which simply stopped. Accordingly, in the most frequent event topology the proton had $\theta < 45°$.

The single-tag trigger for the older sample required a substantial energy deposition in the NaI or shower counter coincident with hits in the IDC, and for low angle tags at least one ODC hit. For the newer sample, the trigger required one clear TPC track with $\theta > 30°$ in coincidence with an energy deposition in either tagging calorimeter, regardless of tag angle. This improved the trigger efficiency at low values of $Q^2$.

In the analysis, we selected events with two oppositely charged tracks coming from the vertex. Both tracks were required to have $\theta > 30°$ (20°) for the untagged (tagged) data and momentum uncertainty less than 50%. Additional nonvertex tracks were allowed. Tags were required to have $E > 6$ GeV and reconstructed tracks in the forward drift chambers. For particle identification, we used an algorithm which compares the measured $dE/dx$ (defined as the average of the lowest 65% of the samples) and momentum to empirically determined curves for the various particle types $(e,\mu,\pi,K,p)$ and determines a $\chi^2$ for each. We required that the proton $\chi^2$ be less than 4 for each track, and smaller than any other $\chi^2$. We also used the sum of the $\chi^2$'s to reject lepton and meson pairs by requiring $\sum \chi_p^2 + 12 < \sum \chi_i^2$ where $i = e,\mu,\pi$ and $\sum \chi_p^2 + 6 < \sum \chi_K^2$. The final results are not sensitive to the details of these cuts. No background from beam-gas events remained after these cuts.

We find 75 untagged and 26 tagged events which pass the above cuts and also an initial cut of $|\sum \mathbf{p}_T| < 0.8$ GeV/$c$ (including the tag, when present). To ensure the exclusivity of these events, we visually scanned them. Events were removed if they had either charged tracks coming from the vertex but not found by the reconstruction algorithms (typically at small angles), or energy depositions in the HEX or pole-tip calorimeters not associated with the tracks. Antiproton annihilation in the coil frequently results in the presence of significant energy depositions far from the track. We avoided rejecting such ambiguous events since any remaining nonexclusive background is later subtracted, as described below. After the scan, 50 untagged and 12 tagged events remained. In Figs. 1(a) and 1(b) we plot $dE/dx$ versus momentum for these event samples. Expected curves for the various particle species are drawn as solid lines. The $\chi^2$ cuts are reflected in this plot; note that the overlap regions do not show any excess, indicating clean samples.

In Figs. 2(a) and 2(b) we show the $|\sum \mathbf{p}_T|^2$ distributions of the untagged and tagged samples. Also shown as curves are the distributions from a Monte Carlo simulation of $e^+e^- \to e^+e^- p\bar{p}$. Events rejected in the scan as nonexclusive show a flat distribution in $|\sum \mathbf{p}_T|^2$ up to 0.3 $(\mathrm{GeV}/c)^2$, consistent with the expectation for events with missing particles. A sample of untagged $\gamma\gamma \to p\bar{p}\pi^+\pi^-$ data was also consistent with a flat distri-

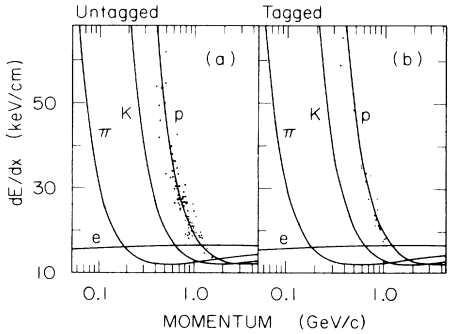


FIG. 1. Truncated mean energy loss vs momentum for particles in the untagged (a) and tagged (b) samples after scanning.

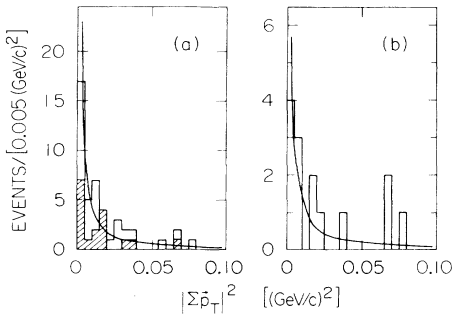


FIG. 2. $|\sum \mathbf{p}_T|^2$ distributions for events passing the scan (histograms) and for Monte Carlo events (solid curves): (a) untagged (5 events off scale), (b) tagged. The shaded region in (a) is the distribution for events in the range $2.0 < W < 2.2$ GeV.

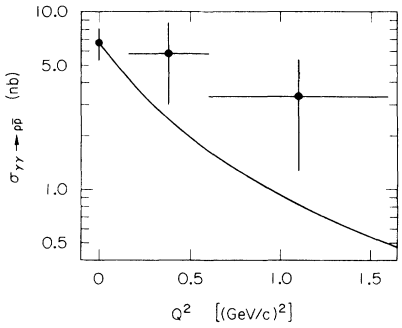


FIG. 4. $Q^2$ dependence of the cross section for $2.0 < W < 2.4$ GeV and $|\cos\theta^*| < 0.6$ The curve is a $\rho$-pole form factor, normalized to the untagged point. Errors are statistical only.

bution when just the $p\bar{p}$ system was considered. We therefore fit the data in Fig. 2(a) [i.e., below 0.1 (GeV/$c$)$^2$] to the sum of the Monte Carlo distribution and a flat background. With a cut at 0.04 (GeV/$c$)$^2$, we find 41 untagged events, with a $W$-independent background of about 8% (Ref. 13). We used a cut of $|\sum \mathbf{p}_T|^2 < 0.05$ (GeV/$c$)$^2$ (including the tag) for the tagged sample, yielding 11 events, with an estimated background of 10% (based on the fit to the untagged data).

To determine the detector acceptance, Monte Carlo events were generated according to the luminosity function for transversely polarized photons.[14] The generated cross section $d\sigma/d|\cos\theta^*|$ was taken to be independent of $W$, $Q^2$, and $\cos\theta^*$. Generated events were run through a detector simulation (which included resolution effects, energy loss, multiple scattering, and nuclear interactions in the detector materials) and then through the same cuts as the data. The events were also subjected to detailed simulations of the untagged and single-tag triggers, including the probabilities (as functions of $p_T$) for ODC hits associated with the tracks. The probability for a proton to have an ODC hit was empirically determined using a sample of inclusive single-tagged events (triggered independently of the ODC) with a $\pm 7°$ matching window in $\phi$. For antiprotons, a Monte Carlo calculation which included annihilation was used to determine the ODC hit probability within $\pm 30°$ in $\phi$, the larger window approximating the trigger requirement. The calculation agrees well with the inclusive antiproton data when a $\pm 7°$ $\phi$ cut is applied.[15]

The same detector simulation was also used for events of the type $e^+e^- \to e^+e^-l^+l^-$ ($l = e,\mu,\tau$), generated according to lowest-order QED (Ref. 16). The total background from these processes is less than 1 event, except for the untagged $e^+e^-e^+e^-$ final state at $W$ above 3.0 GeV (with the particles assigned proton masses). In the range $3.0 < W < 3.5$ GeV, the Monte Carlo simulation predicts $2 \pm 1$ such events in the final sample. There is a single (untagged) event in our final sample in this region; we therefore present the $p\bar{p}$ cross section in the limited range $2.0 < W < 2.8$ GeV.

The cross sections were extracted by comparing the number of background-subtracted data events with the number expected from Monte Carlo simulation (for a given $\gamma\gamma$ cross section) in two-dimensional bins of $W$ and $|\cos\theta^*|$. For the tagged data, this procedure was carried out in two bins of $Q^2$. Figure 3(a) shows the untagged cross section as a function of $W$, integrated over $|\cos\theta^*| < 0.6$. (For $W$ between 2.0 and 2.1 GeV, we

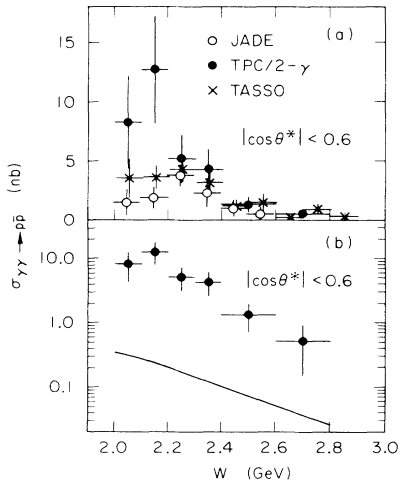


FIG. 3. Untagged cross section for $|\cos\theta^*| < 0.6$, with statistical errors only. (a) compares this measurement with those of Refs. 9 and 10, (b) compares to a curve based on Ref. 7, as described in the text.

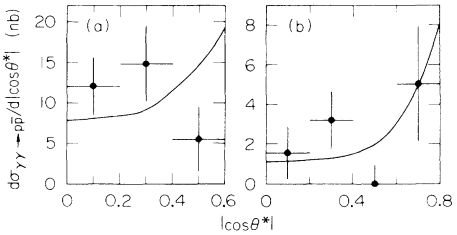


FIG. 5. Angular distributions of the untagged sample for (a) $2.1 < W < 2.4$ GeV, and (b) $2.4 < W < 2.8$ GeV. The curves are QCD predictions. Errors are statistical only.

have acceptance only for $|\cos\theta^*| < 0.3$ and extrapolate to 0.6 assuming an isotropic distribution.) The estimated systematic uncertainty is 20%, with the largest contributions coming from the detector and trigger simulations (in particular the simulation of ODC hits); smaller contributions come from the scan, background subtraction, and luminosity estimate. We also show the cross sections from the TASSO (Ref. 9) and JADE (Ref. 10) measurements. There is some disagreement in the two lowest $W$ bins; over the rest of the spectrum, all the measurements are in good agreement. Figure 3(b) shows our cross section compared to a QCD prediction[7] which we discuss below. In Fig. 4 we present the $Q^2$ dependence of the cross section for $2.0 < W < 2.4$ GeV and $|\cos\theta^*| < 0.6$. Eight of the tagged events are in this region. None of these events had tags with $1.6 < Q^2 < 7$ $(\mathrm{GeV}/c)^2$, leading to a 90%-confidence-level upper limit of 4.1 nb in this $Q^2$ range. The untagged point in Fig. 4 has been adjusted to the same mean $W$ (2.20 GeV) as the tagged points. We estimate the systematic uncertainty for the tagged data to be 20%. The cross section does not fall as steeply as a $\rho$-pole form factor, but the statistics are too limited to make a definitive statement.

The curve in Fig. 3(b) is based on QCD (Ref. 7), where the proton wave function used in the calculation is derived from QCD sum rules.[17] The coupling-constant parameters[18] are estimated from calculations of $B(\psi \to p\bar{p})/B(\psi \to e^+e^-)$, and proton and neutron form factors. Dimensional counting implies $d\sigma/dt \propto W^{-12}$, where $t$ is the square of the four-momentum transferred from photon to hadron; after integration over $\cos\theta^*$ this yields $\sigma(W) \propto W^b(1-4m_p{}^2/W^2)^{1/2}$, with $b = -10$. Even at $W$ above 2.3 GeV (where most $|t|$ values are above 1 $\mathrm{GeV}/c^2$), the prediction lies well below the data. However, the shapes are similar: the best fit of the data to the above $\sigma(W)$ with the normalization and power-law dependence as free parameters yields a value of $b = -13.2 \pm 2.3$. While this is consistent with the value of $-10$ predicted, the larger magnitude and steeper fall of the data may indicate that additional processes (such as resonance production) contribute at low $W$.

In Figs. 5(a) and 5(b) we compare the untagged angular distribution $d\sigma/d|\cos\theta^*|$ in two bins of $W$ to the shapes expected from the same QCD calculation. The curves have been normalized to the number of data events in each bin. In the higher $W$ bin we have acceptance to 0.8 in $|\cos\theta^*|$. In both bins, the data are consistent with flat distributions, but the predicted shapes are not ruled out. The higher $W$ bin appears more consistent with the prediction.

Even with our limited statistics, it is clear that there is considerable disagreement between theory and experiment. However, the steep drop with $W$ and the angular distribution in the higher $W$ bin are at least compatible with the prediction as described above. Among the possible explanations for the discrepancies between theory and measurement are (1) the incomplete understanding of the proton wavefunction, (2) inapplicability of the theory at relatively low-$t$ values, and (3) resonance production. Resolution of these questions requires improved statistics and an increase in the measured $W$ range.

We thank the PEP staff for their dedication and productive running of the machine, and our engineers and technicians for their efforts in the construction and maintenance of the detector. This work was supported in part by the U.S. Department of Energy, the National Science Foundation, the Joint Japan-United States Collaboration in High Energy Physics, and the Foundation for Fundamental Research on Matter in The Netherlands.

[1]S. J. Brodsky and G. P. Lepage, Phys. Rev. D **24**, 1808 (1981).
[2]Ch. Berger *et al.*, Z. Phys. C **26**, 199 (1984).
[3]J. Boyer *et al.*, Phys. Rev. Lett. **56**, 207 (1986).
[4]H. Aihara *et al.*, Phys. Rev. Lett. **57**, 404 (1986).
[5]P. H. Damgaard, Nucl. Phys. **B211**, 425 (1981).
[6]G. Farrar *et al.*, Nucl. Phys. **B259**, 702 (1985); **B263**, 746(E) (1986).
[7]G. Farrar, in *Proceedings of the VI International Workshop on Photon-Photon Collisions*, Lake Tahoe, California, 1984, edited by R. L. Lander (World Scientific, Singapore, 1985), p. 29.
[8]D. Millers and J. Gunion, Phys. Rev. D **34**, 2657 (1986).
[9]M. Althoff *et al.*, Phys. Lett. **130B**, 449 (1983).
[10]W. Bartel *et al.*, Phys. Lett. B **174**, 350 (1986); **178**, 457(E) (1986).
[11]H. Aihara *et al.*, IEEE Trans. Nucl. Sci. **NS-30**, 63 (1983); **NS-30**, 67 (1983); **NS-30**, 76 (1983); **NS-30**, 117 (1983); **NS-30**, 153 (1983).
[12]M. P. Cain *et al.*, Phys. Lett. **147B**, 232 (1984).
[13]The $|\sum \mathbf{p}_T|^2$ spectrum for $2.0 < W < 2.2$ GeV, shown by the shaded portion of Fig. 2(a), is consistent with this same level of background.
[14]V. M. Budnev *et al.*, Phys. Rep. **15**, 182 (1974).
[15]If a $\pm 7°$ $\phi$ cut is applied to the $p\bar{p}$ data and the empirical antiproton ODC hit probability is used in the trigger simulation, cross sections are unchanged within 15%.
[16]J. Smith *et al.*, Phys. Rev. D **15**, 3267 (1977).
[17]V. L. Chernyak and I. R. Zhitnitsky, Nucl. Phys. **B246**, 52 (1984).
[18]The choice of parameters (using the solid curve of Fig. 3, Ref. 7 for $d\sigma/dt$) is as suggested by G. Farrar (private communication).